Stiffness Modeling and Analysis of a Novel 5-DOF Hybrid Robot

Chenglin Dong [a], Haitao Liu [a, *], Wei Yue [a], and Tian Huang [a, b]

[a] *Key Laboratory of Mechanism Theory and Equipment Design of Ministry of Education, Tianjin University, Tianjin 300072, China*
[b] *School of Engineering, The University of Warwick, Coventry CV4 7AL, UK*

Abstract: This paper deals with the stiffness modeling and analysis of a novel 5-DOF hybrid robot named TriMule which is composed of a 3-DOF positioning parallel mechanism plus a 2-DOF wrist. The robot is especially designed as a compact yet rigid module suitable for large part on-site machining. Mainly drawing on screw theory, a semi-analytic stiffness model of the robot is formulated by taking into account the component compliances associated with the elements of both the parallel mechanism and the wrist, resulting in the Cartesian stiffness matrix that can explicitly be expressed in terms of the compliance matrices down to the joint and link level. The stiffness distributions of the tool head over a prescribed task workspace are predicted and the contributions of joint/link compliances are evaluated using a set of global indices.

Key words: Stiffness modeling; Screw theory; Hybrid robot

1 Introduction

In recent years, it has witnessed high demands for large parts in several growing industrial sectors such as aeronautics, astronautics, railroad, and shipping, etc. [1]. The classical and most frequently solution to machining very large parts is to build very large machine tools with serial travels. However, machine tools having large footprints are not suitable for the circumstances where the essential tasks are the on-site machining of relatively small features scattered in several distinct areas on large parts, hole drilling on skin of an aircraft wing, window cutting of wagon panel of a locomotive carriage, for example. A feasible and cost-effective solution is to employ a full 5-DOF (degree-of-freedom) hybrid kinematic machine [2] (or hybrid robot) which can be built as a plug-and-play robotized module mounted on a long reference track such that it can be rapidly and exactly located in the area where machining needs to be performed in situ. This statement can be exemplified by the very successful applications of the Tricept robot [3], which combines three translational parallel axes plus two serial rotary axes, allowing high rigidity and dynamic response to be achieved within a relatively large work envelope. Similar solution of large volume machine tools with hybrid architectures is the Exechon robot [4] proposed by the same inventor of the Tricept.

Stiffness is one of the most important performances of the above-mentioned hybrid robots when they are applied for high-speed machining, where high rigidity and high accuracy are crucially required. Motivated by these requirements, the last two decades have seen tremendous efforts towards this topic [5-19] by taking the Tricept robot as the most widely studied subject [5-15]. For instance, Joshi and Tsai [5] compared the stiffness characteristics of the 3-DOF parallel mechanism within the Tricept robot with that of a 3-DOF manipulator having three supporting legs by merely considering the actuation compliances. Zhang and Gosselin [6-9] proposed the concept of "virtual joint" for stiffness modeling by considering the bending and torsional compliances of the properly constrained passive limb. Wang *et al.* [12] employed the overall Jacobian to formulate the stiffness model by taking into account the compatibility conditions of the passive limb. More recently, Wang *et al.* [15] proposed a stiffness performance index for kineto-elastic statics analysis of parallel mechanism by which the structural optimization issue of the Tricept robot under heavy-load working conditions was investigated. As for the Exechon robot, it seems that Li *et al* [16] were first to present an analytical stiffness model using screw theory and the principle of virtual work. Bi [17] formulated stiffness matrix of the Exechon X700 by which the bearings of both axial and torsional compliances of the actuated limbs on compliance of the end-effector were revealed. By exploring the substructure synthesis technique, Zhang *el al*. [18] developed a stiffness model by taking into account the compliances of both actuated and passive joints as well as limb structures, leading to a parametric analysis

* Corresponding author.
E-mail addresses: liuht@tju.edu,cn

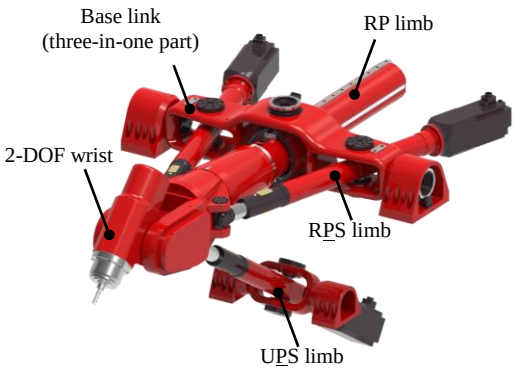

Fig. 1. 3D model of the TriMule robot

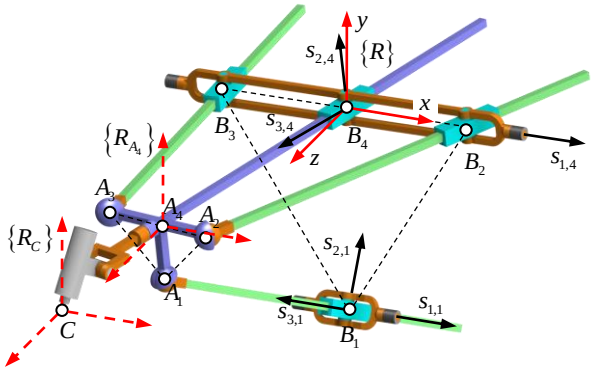

Fig. 2. Schematic diagram of the TriMule robot

that provides useful information for the structural optimization and rigidity improvement. Wang *et al.* [19] developed a stiffness model by taking into account gravitational effects of the movable components of a 5-DOF hybrid robot similar to the Exechon robot. Stiffness modeling, analysis and optimization of various other parallel kinematic machines designed for large part machining were also studied in [20-24].

Driven by the motivation to develop new robotic structures competitive to the well-established Tricept and Exechon, a novel 5-DOF hybrid robot named TriMule was proposed in [25, 26] (see Fig. 1), which is composed of a 3-DOF R(2-R<u>P</u>S&RP)&U<u>P</u>S parallel mechanism plus a A/C wrist. Here, R, P, U, and S represent revolute, prismatic, universal, and spherical joints, respectively; and the underlined <u>P</u> denotes an actuated prismatic joint. The parallel mechanism comprises a spatial limb plus a 2-R<u>P</u>S&RP planar linkage, connected by a pair of R joints to the machine frame at either side of the base link which is elaborately designed into a three-in-one part. This feature brings a special issue that the compliance compatibility conditions amongst three planar limbs must be taken into account in the semi-analytic stiffness modeling of the parallel mechanism. The reminder of this paper is organized as follows. Having addressed the significance of stiffness modeling and given brief introduction to the TriMule robot, Section 2 presents the semi-analytic stiffness modeling strategy and procedure of the TriMule robot with particular interests in dealing with the compliance compatibility arising from the three-in-one part design, resulting in the Cartesian stiffness matrices of both the 3-DOF parallel mechanism and the A/C wrist explicitly expressed in terms of the compliance matrices down to the joint and link level. In Section 3, an example is given to illustrate the effectiveness of the proposed approach with an insight into the contributions of joint/link compliances to the rigidity of the tool head over a prescribed task workspace before conclusions are drawn in Section 4.

2. Stiffness Modeling

In this section we will present a semi-analytic approach for stiffness modeling of the TriMule robot by taking into account compliances of all components. Each component is either a link or 1-DOF revolute or prismatic joint. Moreover, since the stiffness modeling issue is merely considered here, we assume that compliances of a joint are linearly elastic in nature although they would exhibit nonlinear and asymmetrical behaviors under high dynamic loads.

In order to facilitate the semi-analytic stiffness model down to the joint and link level, several frames are placed as shown in Fig.2. A reference frame $\{R\}$ is placed at point B_4, the center of the R joint of the RP limb, with its *y*-axis perpendicular to $\overbrace{B_2B_3}$ and *z*-axis normal to $\Delta B_1B_2B_3$, where point B_1 is the centre of U joint of the U<u>P</u>S limb and B_i $(i=2,3)$ is the centre of R joint of the R<u>P</u>S limb, respectively. To evaluate the externally applied $\$_w$ (expressed in ray-coordinate) wrench and its induced deformation twist $\$_t$ (expressed in axial-coordinate), an instantaneous frame $\{R_C\}$ is placed at the tool tip C with its three axes remaining parallel to those of $\{R\}$. Analogously, an instantaneous frame $\{R_{A_4}\}$ with the same orientations is attached to point A_4 that is the intersection of the axial axis of the passive limb and its normal plane in which all centers of S joints, point A_i $(i=1,2,3)$, are placed. Moreover, the components of

the robot are grouped into a set of elastic elements as given in Appendix A, where a body-fixed frame $\{R_{m_i,i}\}$ attached to the m_ith element of limb i ($i=1,2,3,4$) is placed for evaluating the component compliance.

Fig. 3 shows the elastic system of the TriMule robot, where compliances of all joints and links are taken into account. It is easy to see that the 3-DOF parallel mechanism within the robot can be further decomposed into two sub-chains, i.e. a UPS limb and a 2-RPS&RP planar linkage whose base link is connected by a common rear R joint with the machine frame. In order to facilitate stiffness modeling of such a system using the technique developed in [27], we treat the 2-RPS&RP planar linkage as a 2-DOF actuated compound joint (see Fig. 4) [28] by taking into account the compatibility conditions of three limbs situated on the base link. This special treatment leads to an equivalent 3-DOF parallel mechanism containing two actuated limbs as shown in Fig. 5. In this way, stiffness of the compound joint can be

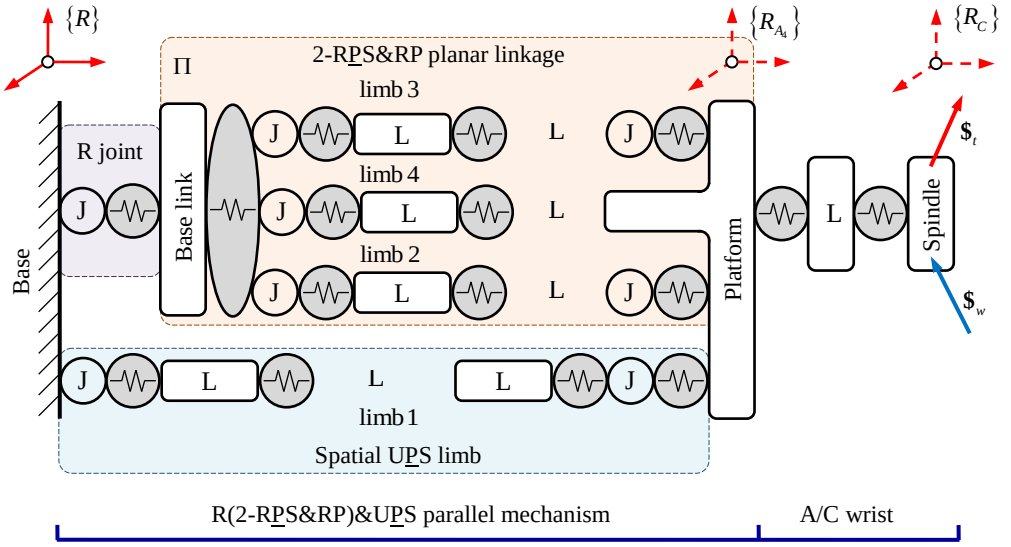

Fig. 3. Elastic model of the TriMule robot

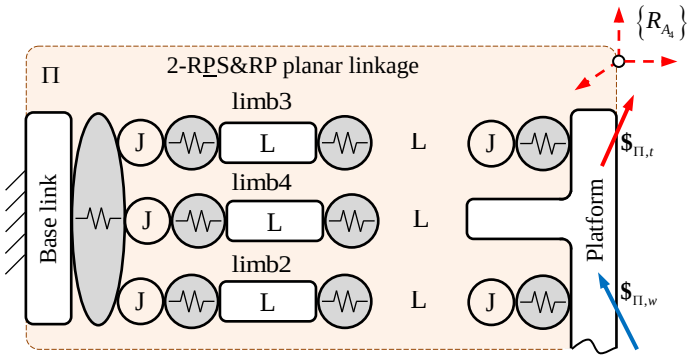

Fig. 4. Elastic model of the 2-RPS&RP compound joint

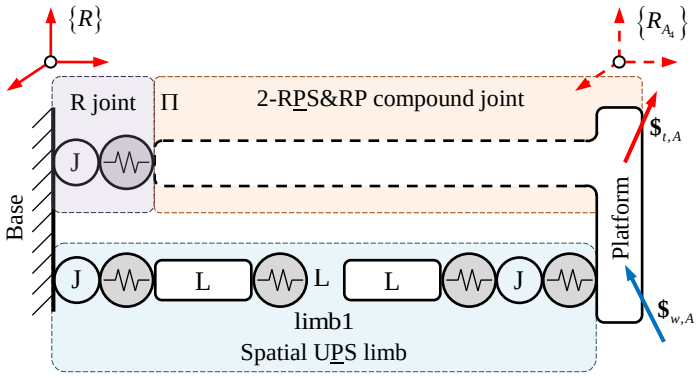

Fig. 5. Elastic model of the equivalent mechanism

formulated first, leading to the stiffness model of the 3-DOF parallel mechanism that can eventually be built by the method developed in [27]. Then, the stiffness model of the robot as a whole can be obtained with easy by means of the superposition principle because all considered subsystems are assumed to be linearly elastic in nature.

1) Stiffness modeling of the compound joint

As shown in Fig. 4, the 2-RPS&RP planar linkage consists of a base link, a platform and three limbs. Stiffness modeling of the base link will be investigated with particular interest by taking into account the compatibility conditions amongst three limbs. Without considering compliance of the three limbs for the time being, the deflection twist of each limb, denoted by $\$_{\Pi,t,b}$, can be decomposed into two components because they share the same platform

$$\$_{\Pi,t,b} = \$^{e}_{\Pi,t,i} + \$^{d}_{\Pi,t,i}, \quad i = 2,3,4 \tag{1}$$

where $\$^{e}_{\Pi,t,i}$ denotes the deflection twist caused by the deflection of the base link at point B_i; $\$^{d}_{\Pi,t,i}$ represents the rigid body motion produced by the idle motions of all passive joints in limb i for meeting the compliance compatibility conditions when all actuated joints are locked.

On one hand, $\$^{e}_{\Pi,t,i}$ can further be expressed as

$$\$^{e}_{\Pi,t,i} = \boldsymbol{T}_{2,i}\$_{t,b,i}, \quad i = 2,3,4 \tag{2}$$

where $\$_{t,b,i}$ denotes the deflection twist of the base link at point (or node) B_i, $\boldsymbol{T}_{2,i}$ denotes the adjoint transformation matrix of $\{R_{2,i}\}$ with respect to $\{R_{A_4}\}$.

On the other hand, note that the wrench system imposed upon the platform does not do work on the rigid body motion produced by the idle motions of the passive joints, the following relationship holds

$$\boldsymbol{W}_i^{\mathrm{T}}\$^{d}_{\Pi,t,i} = 0, \quad i = 2,3,4 \tag{3}$$

$$\boldsymbol{W}_i = \left[\hat{\$}_{wa,i} \quad \hat{\$}_{wc,i}\right], \ \hat{\$}_{wa,i} = \begin{pmatrix} \boldsymbol{s}_{3,i} \\ \boldsymbol{a}_i \times \boldsymbol{s}_{3,i} \end{pmatrix}, \ \hat{\$}_{wc,i} = \begin{pmatrix} \boldsymbol{s}_{2,i} \\ \boldsymbol{a}_i \times \boldsymbol{s}_{3,i} \end{pmatrix}, \ i = 2,3$$

$$\boldsymbol{W}_4 = \left[\hat{\$}_{wc,1,4} \quad \hat{\$}_{wc,2,4} \quad \hat{\$}_{wc,3,4} \quad \hat{\$}_{wc,4,4}\right], \ \hat{\$}_{wc,1,4} = \begin{pmatrix} \boldsymbol{n}_{1,4} \\ -q_{3,4}\boldsymbol{s}_{2,4} \end{pmatrix}, \ \hat{\$}_{wc,2,4} = \begin{pmatrix} \boldsymbol{s}_{2,4} \\ q_{3,4}\boldsymbol{n}_{1,4} \end{pmatrix}, \ \hat{\$}_{wc,3,4} = \begin{pmatrix} \boldsymbol{0} \\ \boldsymbol{s}_{1,4} \end{pmatrix}, \ \hat{\$}_{wc,4,4} = \begin{pmatrix} \boldsymbol{0} \\ \boldsymbol{n}_{3,4} \end{pmatrix}$$

$$\boldsymbol{n}_{1,4} = \boldsymbol{s}_{2,4} \times \boldsymbol{s}_{3,4}, \quad \boldsymbol{n}_{3,4} = \boldsymbol{s}_{1,4} \times \boldsymbol{s}_{2,4}$$

where $\boldsymbol{W}_i$ denotes the matrix formed by the unit wrenches of actuations and/or constraints, denoted by $\hat{\$}_{wa,i}$ and $\hat{\$}_{wc,i}$ ($i = 2,3$) for the RPS limb and by $\hat{\$}_{wc,j_c,4}$ ($j_c = 1,2,3,4$) for the RP limb. Meanwhile, $\boldsymbol{s}_{j_a,i}$ is the unit vector of the j_a th joint axis of limb i and $q_{3,4} = \|\overrightarrow{B_4A_4}\|$.

Hence, substituting Eqs. (2) and (3) into Eq.(1) and followed by taking inner product with $\boldsymbol{W}_i$ on both sides yields the compliance compatibility condition between $\$_{\Pi,t,b}$ and $\$_{t,b,i}$

$$\boldsymbol{W}_i^{\mathrm{T}}\$_{\Pi,t,b} = \boldsymbol{W}_i^{\mathrm{T}}\boldsymbol{T}_{2,i}\$_{t,b,i}, \quad i = 2,3,4 \tag{4}$$

Rewriting Eq. (4) in matrix form gives

$$\$_{\Pi,t,b} = \boldsymbol{J}_{\Pi,b}\left(\$^{\mathrm{T}}_{t,b,2} \quad \$^{\mathrm{T}}_{t,b,3} \quad \$^{\mathrm{T}}_{t,b,4}\right)^{\mathrm{T}} \tag{5}$$

$$\boldsymbol{J}_{\Pi,b} = \left(\boldsymbol{W}_{\Pi}^{\mathrm{T}}\right)^{+}\mathrm{diag}\left[\boldsymbol{W}_i^{\mathrm{T}}\boldsymbol{T}_{2,i}\right], \ \boldsymbol{W}_{\Pi} = \left[\boldsymbol{W}_2 \quad \boldsymbol{W}_3 \quad \boldsymbol{W}_4\right]$$

where $\left(\boldsymbol{W}_{\Pi}^{\mathrm{T}}\right)^{+}$ is the pseudo-inverse of $\boldsymbol{W}_{\Pi}^{\mathrm{T}}$; $\boldsymbol{J}_{\Pi,b}$ is a 6×18 matrix. Indeed, Eq. (5) establishes the relationship between the deflections of the platform evaluated in $\{R_{A_4}\}$ and those at B_i ($i=2,3,4$) evaluated in $\{R_{2,i}\}$.

Evaluated in $\{R_{2,i}\}$, let $\$_{w,b,i}$ ($i=2,3,4$) be the reaction wrenches imposed at B_i. Then, the Hooker's law gives

$$\left(\$_{t,b,2}^{\mathrm{T}} \quad \$_{t,b,3}^{\mathrm{T}} \quad \$_{t,b,4}^{\mathrm{T}}\right)^{\mathrm{T}} = \boldsymbol{K}_{2,4}^{-1}\left(\$_{w,b,2}^{\mathrm{T}} \quad \$_{w,b,3}^{\mathrm{T}} \quad \$_{w,b,4}^{\mathrm{T}}\right)^{\mathrm{T}} \tag{6}$$

where $\boldsymbol{K}_{2,4}^{-1}$ is a 18×18 matrix referred to as the component compliance matrix of the base link. The entries in each column of $\boldsymbol{K}_{2,4}^{-1}$ are the translational/rotational deflections along/about three axes of $\{R_{2,i}\}$ ($i=2,3,4$), which are produced by a unit force/moment along/about these axes. In the semi-analytic stiffness modelling, $\boldsymbol{K}_{2,4}^{-1}$ can directly be generated with the aid of FEA (Finite Element Analysis) software because of its geometric complexity in nature.

Now, let $\$_{\Pi,w}$ be the externally applied wrench imposed upon the platform. Then, the principle of virtual work leads to

$$\$_{\Pi,w}^{\mathrm{T}}\$_{\Pi,t,b} = \sum_{i=2}^{4}\$_{w,b,i}^{\mathrm{T}}\$_{t,b,i} \tag{7}$$

Substituting Eqs. (5) and (6) into Eq. (7) results in the stiffness model of the base link

$$\$_{\Pi,w} = \boldsymbol{K}_{\Pi,b}\$_{\Pi,t,b}, \quad \boldsymbol{K}_{\Pi,b} = \left(\boldsymbol{J}_{\Pi,b}\boldsymbol{K}_{2,4}^{-1}\boldsymbol{J}_{\Pi,b}^{\mathrm{T}}\right)^{-1} \tag{8}$$

where $\boldsymbol{K}_{\Pi,b}$ denotes the stiffness matrix of the base link evaluated in $\{R_{A_4}\}$.

Equipped with Eq. (8) to hand, the stiffness matrix of the compound joint can readily be formulated by simultaneously taking into account the compliances of joints and links within the planar parallel linkage and that of the base link itself. Since the base link and planar linkage are serially connected, the stiffness matrix of this system, denoted by $\boldsymbol{K}_{\Pi}$, can be formulated as

$$\boldsymbol{K}_{\Pi} = \left(\boldsymbol{K}_{\Pi,m}^{-1}+\boldsymbol{K}_{\Pi,b}^{-1}\right)^{-1} \tag{9}$$

$$\boldsymbol{K}_{\Pi,m} = \sum_{i=2}^{4}\boldsymbol{W}_i\bar{\boldsymbol{K}}_i\boldsymbol{W}_i^{\mathrm{T}}, \quad \bar{\boldsymbol{K}}_i = \left(\boldsymbol{W}_i^{\mathrm{T}}\left(\sum_{m_i=3}^{M_i}\boldsymbol{T}_{m_i,i}\boldsymbol{K}_{m_i,i}^{-1}\boldsymbol{T}_{m_i,i}^{\mathrm{T}}\right)\boldsymbol{W}_i\right)^{-1}, \quad M_i = \begin{cases}6 & i=2,3\\ 4 & i=4\end{cases}$$

where $\boldsymbol{K}_{\Pi,m}$ is the stiffness matrix of the planar parallel linkage without considering compliance of the base link. $\boldsymbol{K}_{m_i,i}^{-1}$ is the compliance matrix of element m_i evaluated in its body fixed frame $\{R_{m_i,i}\}$. Note that $\boldsymbol{K}_{m_i,i}^{-1}$ can be generated again using a commercialized FEA software. $\boldsymbol{T}_{m_i,i}$ is the adjoint transformation matrix of $\{R_{m_i,i}\}$ with respect to $\{R_{A_4}\}$. It should be noted that for 1-DOF actuated joint and elastic links, $\boldsymbol{K}_{m_i,i}$ is of full rank and $\boldsymbol{T}_{m_i,i}$ is a 6×6 matrix; otherwise, $\boldsymbol{K}_{m_i,i}$ and $\boldsymbol{T}_{m_i,i}$ with reduced dimensions should be used by considering only the entries associated with the constrained axes. For more information about the formulation of a proper $\boldsymbol{K}_{m_i,i}$ and $\boldsymbol{T}_{m_i,i}$, please refer to [27].

2) Stiffness modeling of the 3-DOF parallel mechanism

Having developed the stiffness matrix of the compound joint given in Eq. (9), the stiffness model of the 3-DOF parallel mechanism can be formulated with case by following the procedure proposed in [27]. Examining the structure of the equivalent mechanism shown in Fig. 5 indicates that the serially connected compound joint and the rear R joint forms one limb, and the UPS limb forms another, both are connected with the platform at one end and with the machine frame at the other. Thus, the stiffness matrix of the 3-DOF parallel mechanism, denoted by $\boldsymbol{K}_{p,A}$, is of the form

$$\boldsymbol{K}_{p,A}=\hat{\$}_{wa,1}\left(\hat{\$}_{wa,1}^{\mathrm{T}}\left(\sum_{m_1=1}^{6}\boldsymbol{T}_{m_1,1}\boldsymbol{K}_{m_1,1}^{-1}\boldsymbol{T}_{m_1,1}^{\mathrm{T}}\right)\hat{\$}_{wa,1}\right)^{-1}\hat{\$}_{wa,1}^{\mathrm{T}}+\boldsymbol{W}_R\left(\boldsymbol{W}_R^{\mathrm{T}}\left(\boldsymbol{T}_{1,4}\boldsymbol{K}_{1,4}^{-1}\boldsymbol{T}_{1,4}^{\mathrm{T}}+\boldsymbol{K}_{\Pi}^{-1}\right)\boldsymbol{W}_R\right)^{-1}\boldsymbol{W}_R^{\mathrm{T}} \tag{10}$$

$$\hat{\$}_{wa,1}=\begin{pmatrix}\boldsymbol{s}_{3,1}\\ \boldsymbol{a}_1\times\boldsymbol{s}_{3,1}\end{pmatrix},\quad \boldsymbol{W}_R=\begin{bmatrix}\hat{\$}_{wc,1,R} & \hat{\$}_{wc,2,R} & \hat{\$}_{wc,3,R} & \hat{\$}_{wc,4,R} & \hat{\$}_{wc,5,R}\end{bmatrix}$$

$$\hat{\$}_{wc,1,R}=\begin{pmatrix}\boldsymbol{s}_{1,4}\\ -q_{3,4}\boldsymbol{s}_{3,4}\times\boldsymbol{s}_{1,4}\end{pmatrix},\ \hat{\$}_{wc,2,R}=\begin{pmatrix}\boldsymbol{s}_{2,4}\\ -q_{3,4}\boldsymbol{s}_{3,4}\times\boldsymbol{s}_{2,4}\end{pmatrix},\ \hat{\$}_{wc,3,R}=\begin{pmatrix}\boldsymbol{n}_{3,4}\\ -q_{3,4}\boldsymbol{s}_{3,4}\times\boldsymbol{n}_{3,4}\end{pmatrix},\ \hat{\$}_{wc,4,R}=\begin{pmatrix}\boldsymbol{0}\\ \boldsymbol{s}_{2,4}\end{pmatrix},\ \hat{\$}_{wc,5,R}=\begin{pmatrix}\boldsymbol{0}\\ \boldsymbol{n}_{3,4}\end{pmatrix}$$

where $\boldsymbol{W}_R$ denotes the matrix formed by the unit wrenches of constraints, $\hat{\$}_{wc,j_c,R}$ ($j_c=1,2,\mathrm{L}\ ,5$), imposed by the rear R joint upon the platform; $\boldsymbol{K}_{1,4}^{-1}$ denotes the component compliance matrix of the rear R joint evaluated in $\{R_{1,4}\}$; and $\boldsymbol{T}_{1,4}$ denotes the adjoint transformation matrix of $\{R_{1,4}\}$ with respect to $\{R_{A_4}\}$. The interpretations of other symbolic notations associated with the spatial UPS in the first term of Eq. (10) can be made according to their counterparts defined in Eq. (9). Obviously, the first and second components in $\boldsymbol{K}_{p,A}$ are respectively the stiffness matrix of the UPS limb, and that of the limb serially formed by the compound joint and the rear R joint.

3) Stiffness modeling of the hybrid robot

Building upon the forgoing stiffness modeling technique, the stiffness matrix, denoted by $\boldsymbol{K}$, of the TriMule robot as a whole can directly be achieved without further derivation. Note that the platform of the 3-DOF parallel mechanism is serially connected with the A/C wrist through a trust bearing, the stiffness matrix of the hybrid robot can then be represented by

$$\boldsymbol{K}=\left(\boldsymbol{K}_p^{-1}+\boldsymbol{K}_s^{-1}\right)^{-1} \tag{11}$$

$$\boldsymbol{K}_p=\boldsymbol{T}_{AC}\boldsymbol{K}_{p,A}\boldsymbol{T}_{AC}^{\mathrm{T}},\quad \boldsymbol{K}_s=\left(\sum_{m_4=5}^{6}\boldsymbol{T}_{m_4,4}\boldsymbol{K}_{m_4,4}^{-1}\boldsymbol{T}_{m_4,4}^{\mathrm{T}}\right)^{-1}$$

where $\boldsymbol{T}_{AC}$ and $\boldsymbol{T}_{m_4,4}$ are the adjoint transformation matrices of $\{R_{A_4}\}$ and $\{R_{m_4,4}\}$ with respect to $\{R_C\}$, respectively; $\boldsymbol{K}_{m_4,4}$ ($m_4=5,6$) is the 6×6 component stiffness matrix evaluated in its body-fixed frames. The explicit expressions of Eqs. (9)-(11) fully embody the strategy and procedure for formulating the stiffness model at down to joint/link level of the TriMule robot as clearly depicted *via* Figs. 3~4.

3. Example

In this section, rigidity of the TriMule 600 robot over a prescribed task workspace is evaluated using the stiffness model developed in Sections 2. In order to make full use of the reachable workspace, the task workspace W_t of point P is defined as the combination of a cylindrical portion and a spherical portion, as shown in Fig. 6. The dimensional parameters of the robot and the prescribed task workspace are shown in Table 1. Evaluated in the corresponding body-fixed frames, Table A-1~A-2 show the component compliance matrices $\boldsymbol{K}_{m_i,i}^{-1}$ calculated by a commercial FEA software SAMCEF [27, 29, 30]. Table A.3 shows the structural parameters of the limb-body assemblies. It should be noted that the component stiffness matrix of the limb-body assembly is generated by polynomial fitting technique because it is configuration-dependent. Meanwhile, the rotational angles of the A/C wrist are set to be $\theta_{4,4}=0$ and $\theta_{5,4}=0$ in the rigidity evaluation.

The four indices proposed in [20] are employed for evaluating the rigidities of the robot because it is especially designed for milling and drilling

$$k_{tx}=1/\boldsymbol{C}'(1,1),\ \ k_{ty}=1/\boldsymbol{C}'(2,2),\ \ k_{tz}=1/\boldsymbol{C}'(3,3),\ \ k_{rz}=1/\boldsymbol{C}'(6,6) \tag{12}$$

$$\boldsymbol{C}'=\left(\begin{bmatrix}\boldsymbol{R}_{6,4} & \boldsymbol{0}\\ \boldsymbol{0} & \boldsymbol{R}_{6,4}\end{bmatrix}^{\mathrm{T}}\boldsymbol{K}\begin{bmatrix}\boldsymbol{R}_{6,4} & \boldsymbol{0}\\ \boldsymbol{0} & \boldsymbol{R}_{6,4}\end{bmatrix}\right)^{-1}$$

where $\boldsymbol{R}_{6,4}$ is the orientation matrix of $\{R_{6,4}\}$ with respect to $\{R_C\}$. These indices can be physically interpreted as the

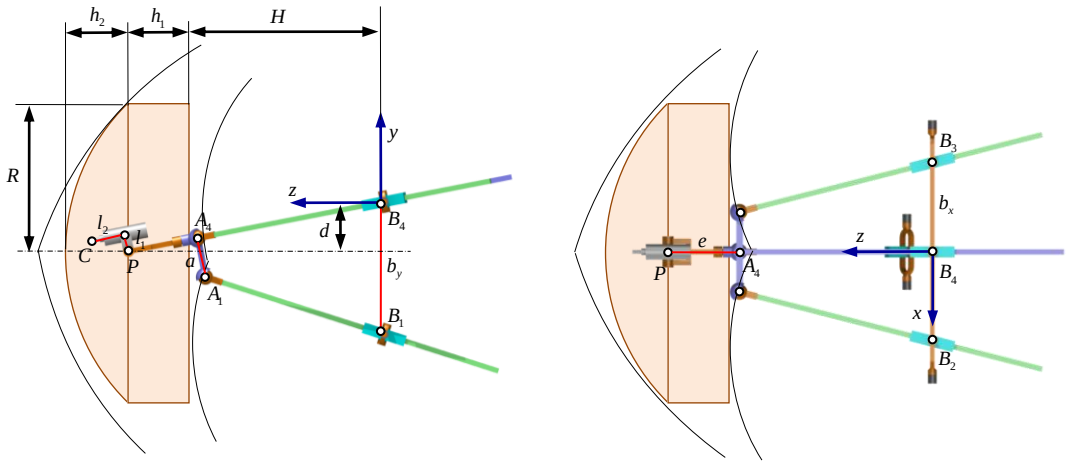

Fig. 6. Task workspace of the TriMule robot

Table 1 Dimensional parameters of the TriMule 600 robot (in meters)

a	b_x	b_y	e	l_1	l_2	d	H	h_1	h_2	R
0.135	0.320	0.570	0.345	0.120	0.220	0.190	1.000	0.240	0.220	0.620

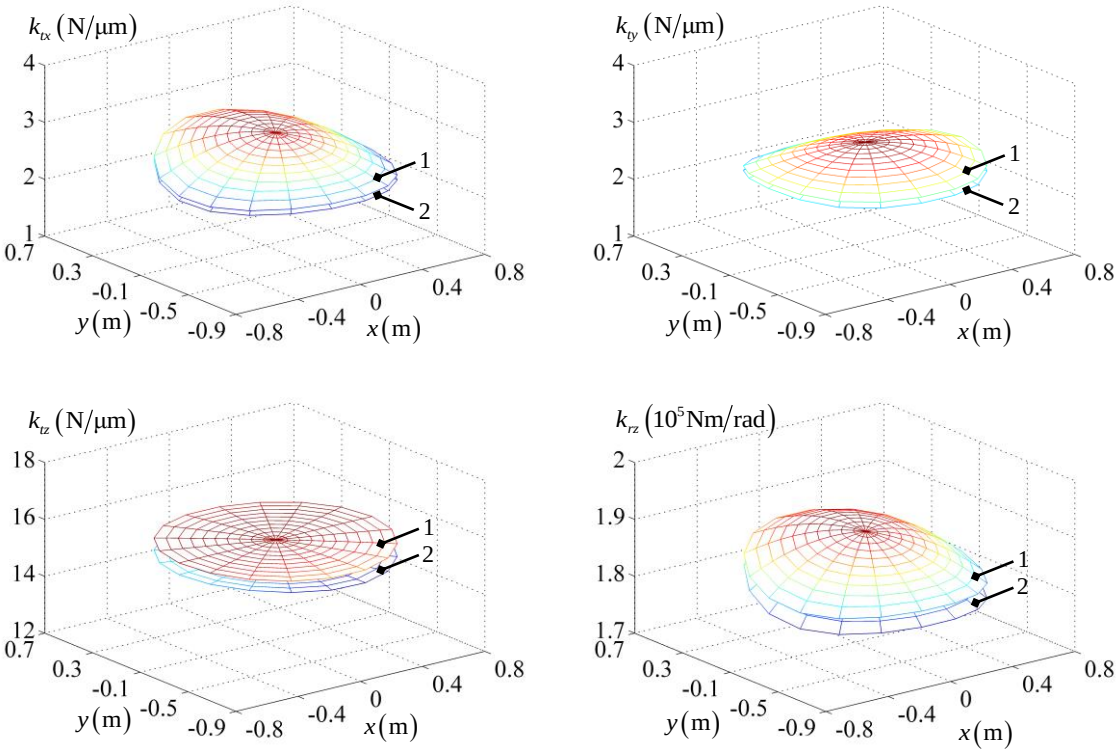

Fig. 7. Stiffness distributions of the TriMule 600 robot at $z=H+h_1$. 1: Semi-analytical model, 2: FEA model

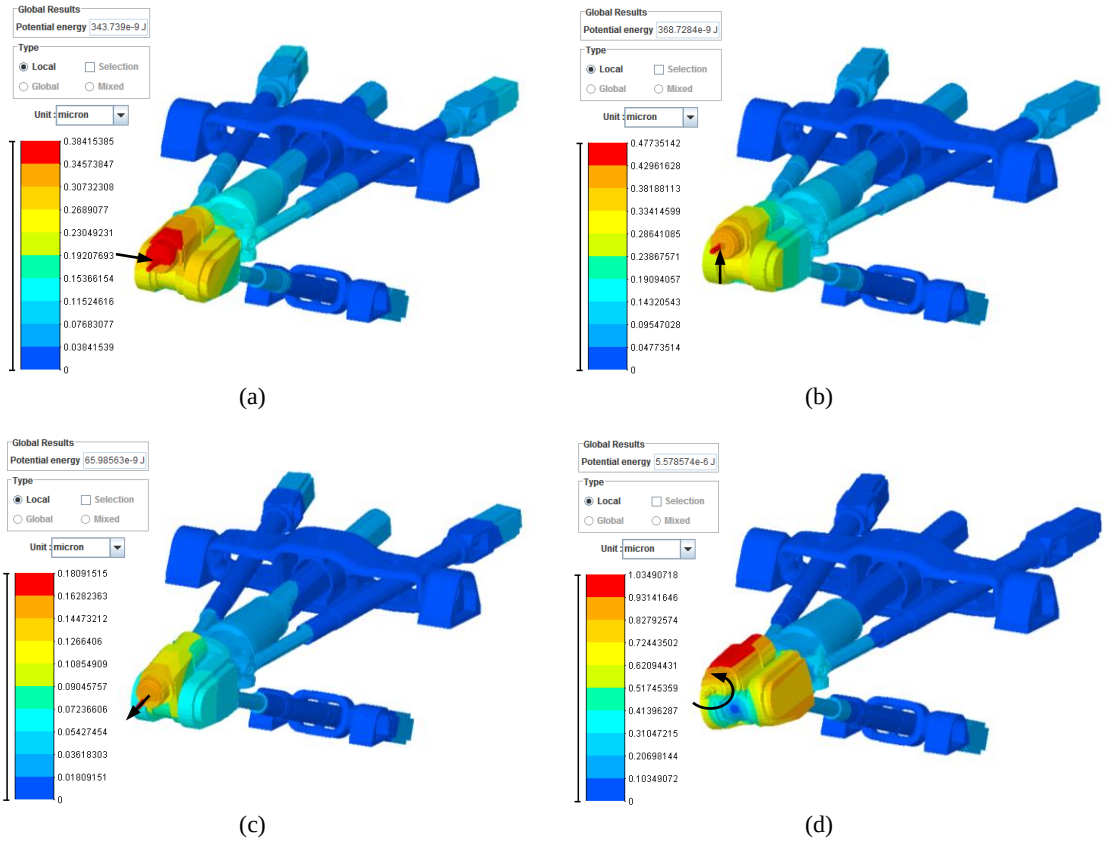

Fig. 8. Elastic deformation of FE model at the reference configuration under unit force/torque: (a) along the $x_{6,4}$ -axis, (b) along the $y_{6,4}$ -axis, (c) along the $z_{6,4}$ -axis, and (d) about the $z_{6,4}$ -axis.

Table 2 Results obtained by the semi-analytic model and FE model at the reference configuration

	$k_{tx}\left(\mathrm{N/\mu m}\right)$	$k_{ty}\left(\mathrm{N/\mu m}\right)$	$k_{tz}\left(\mathrm{N/\mu m}\right)$	$k_{rz}\left(10^5\mathrm{Nm/rad}\right)$
Semi-analytic	3.05	2.88	15.77	1.90
FEA	2.90	2.71	15.15	1.79
Residual	5.17%	6.27%	4.09%	6.15%

linear stiffness along the $x_{6,4}$ -, $y_{6,4}$ -, $z_{6,4}$ -axis and the torsional stiffness about the $z_{6,4}$ -axis.

In order to validate the proposed stiffness model, the deflection analysis is implemented using the commercial software SAMCEF. Fig. 7 shows the distributions of k_{tx}, k_{ty}, k_{tz} and k_{rz} in the middle layer of the task workspace ($z=H+h_1$) obtained by the semi-analytical model and FE model, respectively. Meanwhile, Fig. 8 illustrates the elastic deformation of the FE model at a reference configuration, where $\boldsymbol{r}_P=\begin{pmatrix}0 & -d & H+h_1\end{pmatrix}^{\mathrm{T}}$, $\theta_{4,4}=0$ and $\theta_{5,4}=0$ as shown in Fig. 6. It can be concluded from Fig. 7 and the results given in Table 2 that the elastic deformation obtained by the semi-analytic model match satisfactorily with those obtained by FE model in terms of both magnitude and distribution. Fig. 9 shows distributions of four indices in the $x=0$ layer and $y=-d$ layer of the task workspace. It can be found that: 1) k_{tx}, k_{ty}, k_{tz} and k_{rz} are symmetrically distributed with respect to the $y-z$ plane, and they all decrease with increment of the z coordinate; 2) k_{tx} and k_{ty} are similar in magnitudes, falling into ranges of 2.3~3.9 $\mathrm{N/\mu m}$ and 2.3~3.5 $\mathrm{N/\mu m}$, respectively; 3) the variations of k_{tz} and k_{rz} are relatively small, k_{tz} varies in 15.5~16 $\mathrm{N/\mu m}$, which is approximately 4~6.5 times higher than those of k_{tx} and k_{ty}; while k_{rz} fluctuates within a range of 1.82~2.00$\times10^5$ Nm/rad; 4) the variation of k_{tx} are similar to that of k_{rz}, and their values reach the maximum

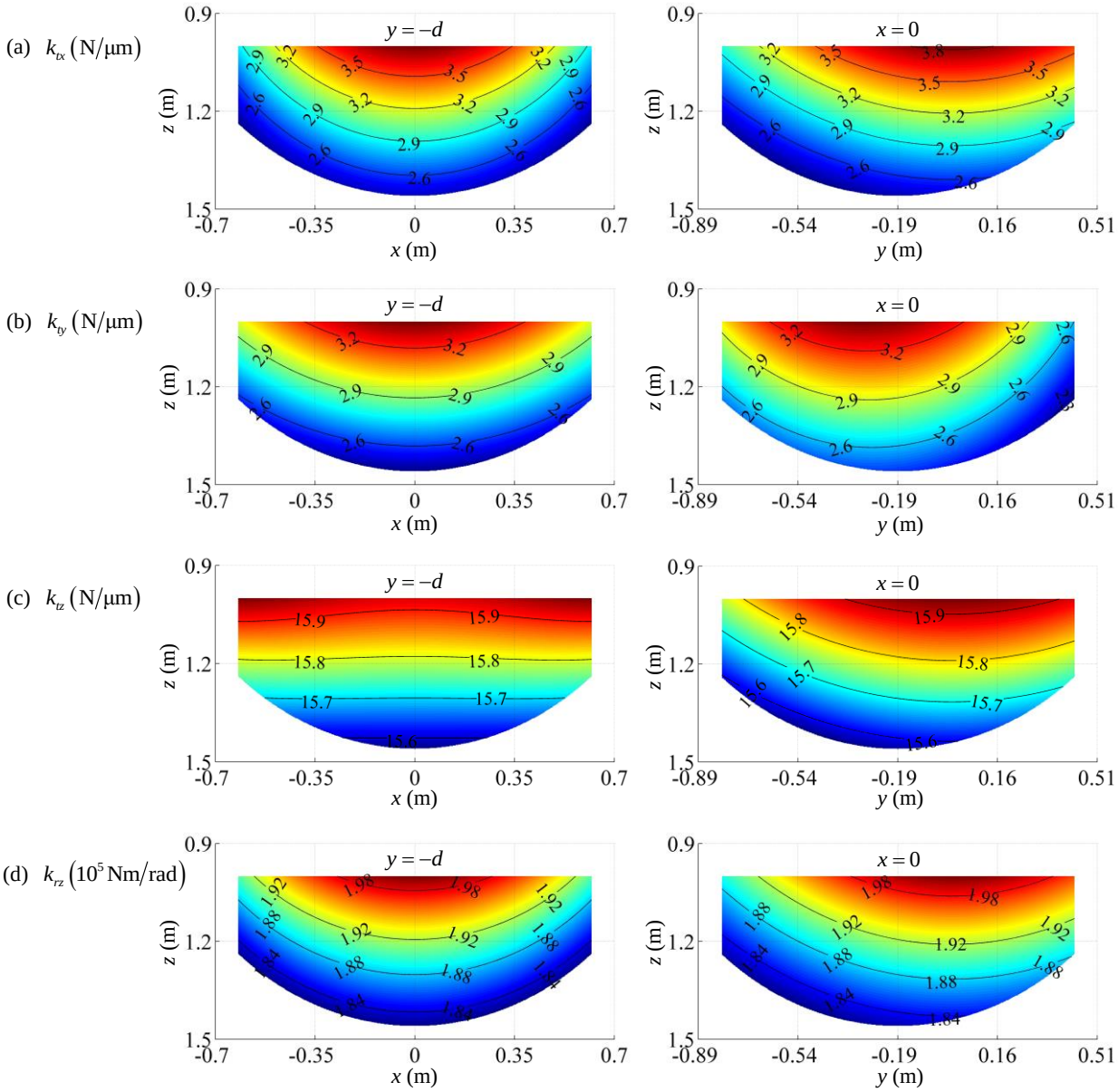

Fig. 9. Stiffness distributions of the TriMule 600 robot in the task workspace

at the configuration $r_P = (0 \quad 0 \quad H)^{\mathrm{T}}$; and 5) k_{ty} takes the maximum value near $r_P = (0 \quad -d \quad H)^{\mathrm{T}}$, while k_{tz} takes the maximum value at the workspace boundary.

To investigate the influences of the component compliances on the tool head rigidity, the following global indices are employed

$$\bar{c}_{tx} = \frac{\int_{W_t} \boldsymbol{C}'(1,1)\, dV}{V}, \quad \bar{c}_{ty} = \frac{\int_{W_t} \boldsymbol{C}'(2,2)\, dV}{V}, \quad \bar{c}_{tz} = \frac{\int_{W_t} \boldsymbol{C}'(3,3)\, dV}{V}, \quad \bar{c}_{rz} = \frac{\int_{W_t} \boldsymbol{C}'(6,6)\, dV}{V} \tag{13}$$

where V represents the volume of W_t. The physical meanings of $\bar{c}_{tx}$, $\bar{c}_{ty}$, $\bar{c}_{tz}$ and $\bar{c}_{rz}$ are the mean values of k_{tx}, k_{ty}, k_{tz} and k_{rz} throughout W_t. The contributions of the component compliances to the global indices are given in Table 3. It can be observed that the compliance of the 2-DOF wrist has relatively significant bearing on the global indices than that of the 3-DOF parallel mechanism (up to 55.09%, 67.28%, 80.83% and 70.94%, respectively). Without considering of the wrist, the compliance of the limb-body assembly of the actuated limbs has relatively significant effect on $\bar{c}_{tx}$, $\bar{c}_{ty}$ and $\bar{c}_{tz}$ (up to 61.36%, 58.89% and 55.61%, respectively); while $\bar{c}_{rz}$ is mainly dominated by the limb-body assembly of the passive limb (up to 80.76%). Therefore, more cares should be excised on the mechanical

Table 3 Contributions of the component compliances to global indices (unit: %)

Global indices	Actuated limbs ($i=1,2,3$)						Passive limb				Wrist	
	$\boldsymbol{K}_{1,1}^{-1}$	$\boldsymbol{K}_{2,1}^{-1}$	$\boldsymbol{K}_{3,i}^{-1}$	$\boldsymbol{K}_{4,i}^{-1}$	$\boldsymbol{K}_{5,i}^{-1}$	$\boldsymbol{K}_{6,i}^{-1}$	$\boldsymbol{K}_{1,4}^{-1}$	$\boldsymbol{K}_{2,4}^{-1}$	$\boldsymbol{K}_{3,4}^{-1}$	$\boldsymbol{K}_{4,4}^{-1}$	$\boldsymbol{K}_{5,4}^{-1}$	$\boldsymbol{K}_{6,4}^{-1}$
$\bar{c}_{tx}$	0	0	2.11	27.56	2.31	3.33	0.68	0.25	0.03	8.64	52.48	2.61
$\bar{c}_{ty}$	1.36	0.86	1.82	19.27	1.88	2.71	2.15	0.28	0.03	2.36	42.76	24.52
$\bar{c}_{tz}$	0	0	1.01	10.66	1.10	1.59	4.32	0.46	0	0.03	19.02	61.81
$\bar{c}_{rz}$	0	0	0.38	3.93	0.02	0.02	0.04	0.25	0.97	23.47	62.41	8.53

design of the 2-DOF wrist and the limb-body assembly of the passive limb in order to achieve a compact yet rigid design.

4. Conclusions

Mainly drawing on screw theory, this paper investigates semi-analytic stiffness modeling of the TriMule robot. The conclusions are drawn as follows.

(1) In order to facilitate the stiffness modeling of R(2-RPS&RP)&UPS parallel mechanism, the 2-RPS&RP planar linkage can be treated as a 2-DOF actuated compound joint, allowing the compliance compatibility conditions to be found first. This special treatment enables the stiffness modeling to be implemented using the standard procedure proposed by [27], resulting in an explicit expression for the Cartesian stiffness matrix in terms of the compliance matrices of all joints/links evaluated in their local body-fixed frames.

(2) The effectiveness of the proposed stiffness model has been verified by a comparison study against FEA software. The results show that sufficient computational accuracy can be achieved for the prediction of stiffness distribution over the task workspace.

(3) The results of stiffness analysis also show that for achieving a light weight yet rigid design more cares should be taken on counterbalancing the rigidities of the A/C wrist and the 3-DOF parallel mechanism, and those of the actuated and passive limb-body assemblies within the parallel mechanism. Moreover, the design method for achieving high dynamic response subject to the rigidity and dexterity constraints is an important issue worthy of investigation. These issues, however, will be reported in separate articles.

Acknowledgments

This work is partially supported by National Natural Science Foundation of China (Grants 51622508 and 51420105007) and EU H2020-RISE-ECSASDP (Grant 734272).

References

[1] L. Uriarte, M. Zatarain, D. Axinte, J. Yagüe-Fabra, S. Ihlenfeldt, J. Eguia, and A. Olarra, "Machine Tools for Large Parts," *Annals of the CIRP*, vol. 62, no. 2, pp. 731-750, 2013.

[2] M. Weck, and D.Staimer, "Parallel Kinematic Machines Tools – Current State and Future Potentials," *Annals of the CIRP*, vol. 51, no. 2, pp. 671-674, 2002.

[3] K. E. Neumann, "Tricept Application," *Proceedings-3rd Chemnitz Parallel Kinematics Seminar*, Zwickau, Germany, pp. 547-551, 2002.

[4] K. E. Neumann, "The Key to Aerospace Automation," *SAE Aerospace Manufacturing and Automated Fastening Conference and Exhibition*, Detroit, USA, Paper No. 2006-01-3144, 2006.

[5] S. Joshi, L. W. Tsai, "A comparison study of two 3-DOF parallel manipulators: one with three and the other with four supporting legs," *IEEE Trans. Robot. Autom.*, vol. 19, no. 2, pp. 200-209, 2003.

[6] C. M. Gosselin, D. Zhang, "Stiffness analysis of parallel mechanisms using a lumped model," *Int. J. Robot. Autom.*, vol. 17, no. 1, pp. 17-27, 2002.

[7] D. Zhang, C. M. Gosselin, "Kinetostatic Modeling of Parallel Mechanisms with a Passive Constraining Leg and Revolute Actuators," *Mech. Mach. Theory*, vol. 37, no. 6, pp. 599-617, 2002.

[8] D. Zhang, C. M. Gosselin, “Kinetostatic Analysis and Design Optimization of the Tricept Machine Tool Family,” *ASME J. Manuf. Sci. Eng.*, vol. 124, no. 3, pp. 725-733, 2002.
[9] D. Zhang, “On stiffness improvement of the Tricept machine tool,” *Robotica*, vol. 23, no. 3, pp. 377-386, 2005.
[10] J.W. Kim, K.W. Kim, H.S. Kim, J.H. Kyung, “Stiffness analysis and design of a 3-DOF parallel robot with one constraining leg,” *Proceedings of the International Conference on Control, Automation and Systems*, Seoul, Korea, pp. 2288–2293, 2007.
[11] Y. Y. Wang, T. Huang, X. M. Zhao, J. P. Mei, “Finite Element Analysis and Comparison of Two Hybrid Robots-the Tricept and the TriVariant,” *IEEE/RSJ International Conference on Intelligent Robots and Systems*, pp. 490-495, 2007.
[12] Y. Wang, H. Liu, T. Huang, D. G. Chetwynd, “Stiffness modeling of the Tricept robot using the overall Jacobian matrix,” *ASME J. Mech. Robot.*, vol. 1, no. 1, pp. 795-810, 2009.
[13] T. Bonnemains, H. Chanal, B. C. Bouzgarrou, P. Ray, “Stiffness computation and identification of parallel kinematicmachine tools,” *J. Manuf. Sci. Eng.*, vol. 131, no. 4, pp. 481-498, 2009.
[14] S. K. Han, “Stiffness of parallel manipulators with serially connected legs,” *ASME J. Mech. Robot.*, vol. 23, no. 2, pp. 164-172, 2014.
[15] H. Wang, L. S. Zhang, G. L. Chen, S. Z. Huang, "Parameter optimization of heavy-load parallel manipulator by introducing stiffness distribution evaluation index," *Mech. Mach. Theory*, vol. 108, pp. 244-259, 2017.
[16] X. Li, D. Zlatanov, M. Zoppi, R. Molfino, “Stiffness estimation and experiments for the Exechon parallel self-reconfiguring fixture mechanism,” *in: Proceedings of the ASME International Design Engineering Technical Conference on Computers and Information in Engineering*, Chicago, Illinois, USA, pp. 637-645, 2012.
[17] Z.M. Bi, “Kinetostatic modeling of Exechon parallel kinematic machine for stiffness analysis,” *Int. J. Adv. Manuf. Technol.*, vol. 71, pp. 325-335, 2014.
[18] J. Zhang, Y. Zhao, Y. Jin, “Kinetostatic-model-based stiffness analysis of Exechon PKM,” *Robot. Comput.-Integr. Manuf.*, vol. 37, pp. 208-220, 2015.
[19] M. Wang, H. Liu, T. Huang, D. G. Chetwynd, “Compliance analysis of a 3-SPR parallel mechanism with consideration of gravity,” *Mech. Mach. Theory*, vol. 84, no. 1, pp. 99-112, 2015.
[20] Y. G. Li, H. Liu, X. M. Zhao, T. Huang, D. G. Chetwynd, “Design of a 3-DOF PKM module for large structural component machining.” *Mech. Mach. Theory*, vol. 45, no.6, pp. 941-954, 2010.
[21] B. Lian, T. Sun, Y. Song, Y. Jin, M. Price, “Stiffness analysis and experiment of a novel 5-DoF parallel kinematic machine considering gravitational effects,” *Int. J. Mach. Tools Manuf.*, vol. 95, pp. 82-96, 2015.
[22] M. X. Wang, H. T. Liu, T. Huang, “An approach for the lightweight design of a 3-SPR parallel mechanism,” *ASME J. Mech. Robot.*, vol. 9, no. 5, pp. 051016-051016-10, 2017.
[23] W. Cao, H. Ding, “A method for stiffness modeling of 3R2T overconstrained parallel robotic mechanisms based on screw theory and strain energy,” *Precision Engineering*, ISSN 0141-6359, 2017.
[24] W. Cao, D. Yang, H. Ding, “A method for stiffness analysis of overconstrained parallel Robotic mechanisms with scara motion,” *Robot. Comput.-Integr. Manuf.*, vol. 49, pp. 426-435, 2018.
[25] T. Huang, C. Dong, H. Liu, X. Qin, J. Mei, Q. Liu, M. Wang, “Five-degree-of-freedom Parallel Robot with Multi-shaft Rotary Brackets,” Pub. No.: WO/2017/005015, 2017-01-12.
[26] C. Dong, H. Liu, Q. Liu, T. Sun, T. Huang, D. G. Chetwynd, “An approach for type synthesis of overconstrained 1T2R parallel mechanisms,” *In Computational Kinematics*. Springer, Cham, pp. 274-281, 2018.
[27] H. Liu, T. Huang, D. G. Chetwynd, A. Kecskeméthy, “Stiffness modelling of parallel mechanisms at limb and joint/link levels,” *IEEE Trans. Robot.*, vol. 33, no. 3, pp. 734-741, 2017.
[28] F. Gao, W. Li, X. Zhao, Z. Jin, H. Zhao, “New kinematic structures for 2-, 3-, 4-, and 5-dof parallel manipulator designs,”. *Mech. Mach. Theory*, vol. 37, no. 11, pp. 1395-1411, 2002.
[29] A. Pashkevich, A. Klimchik, D. Chablat. “Enhanced stiffness modeling of manipulators with passive joints,” *Mech. Mach. Theory*, vol. 46, no. 5, pp. 662-679, 2011.
[30] A. Klimchik, A. Pashkevich, D. Chablat, “CAD-based approach for identification of elasto-static parameters of robotic manipulators,” *Finite Elemement Anal. Des.*, vol. 75, pp. 19–30, 2013.

Appendix A

Table A-1 The body fixed frames and compliance matrixes of the elastic elements in the actuated limb

m_i	$\{R_{m_i,i}\}$	$\boldsymbol{R}_{m_i,i}$, $\boldsymbol{s}_{j_i,i}$, $\boldsymbol{K}_{m_i,i}^{-1}$ (unit: N, m, rad)
1	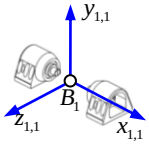 First R joint of the U joint	$\boldsymbol{R}_{1,1}=\boldsymbol{E}_3=\left[\hat{\boldsymbol{x}}_{1,1}\quad\hat{\boldsymbol{y}}_{1,1}\quad\hat{\boldsymbol{z}}_{1,1}\right]$, $\boldsymbol{s}_{1,1}=\hat{\boldsymbol{x}}_{1,1}$, $\boldsymbol{K}_{1,1}^{-1}=\begin{bmatrix}1.07 & -5.71\times10^{-5} & -1.47\times10^{-3} & -2.90\times10^{-3} & -0.26\\ & 2.22 & -4.53\times10^{-3} & 1.12\times10^{-2} & -9.64\times10^{-2}\\ & & 1.25 & 7.07\times10^{-2} & -1.21\times10^{-2}\\ & \text{sym.} & & 82.90 & 0.20\\ & & & & 81.72\end{bmatrix}\times10^{-9}$
2	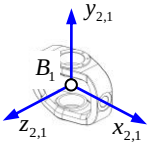 Ring of the U joint	$\boldsymbol{R}_{2,1}=\boldsymbol{R}_{1,1}\mathrm{Rot}\left(x_{1,1},\theta_{1,1}\right)=\left[\hat{\boldsymbol{x}}_{2,1}\quad\hat{\boldsymbol{y}}_{2,1}\quad\hat{\boldsymbol{z}}_{2,1}\right]$ $\boldsymbol{K}_{2,1}^{-1}=\begin{bmatrix}0.56 & 1.09\times10^{-3} & -2.29\times10^{-4} & -9.68\times10^{-3} & -1.62\times10^{-2} & -1.24\times10^{-2}\\ & 0.86 & -1.66\times10^{-3} & -8.10\times10^{-3} & -8.37\times10^{-3} & -1.57\times10^{-2}\\ & & 0.91 & 4.47\times10^{-2} & 1.51\times10^{-2} & 5.24\times10^{-3}\\ & & & 126.27 & -0.27 & -2.15\times10^{-2}\\ & \text{sym.} & & & 50.14 & -1.93\times10^{-2}\\ & & & & & 26.49\end{bmatrix}\times10^{-9}$
3	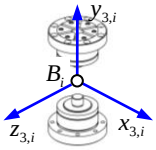 Second R joint of the U joint (or the R joint of RPS limb)	$\boldsymbol{R}_{3,i}=\boldsymbol{R}_{2,i}\mathrm{Rot}\left(y_{2,i},\theta_{2,i}\right)=\left[\hat{\boldsymbol{x}}_{3,i}\quad\hat{\boldsymbol{y}}_{3,i}\quad\hat{\boldsymbol{z}}_{3,i}\right]$, $\boldsymbol{s}_{2,i}=\hat{\boldsymbol{y}}_{3,i}$ $\boldsymbol{K}_{3,i}^{-1}=\begin{bmatrix}1.22 & -1.11\times10^{-3} & 1.69\times10^{-2} & 7.93\times10^{-3} & 0.36\\ & 1.76 & -4.32\times10^{-3} & -5.89\times10^{-2} & 1.23\times10^{-2}\\ & & 1.22 & 0.39 & -7.93\times10^{-3}\\ & \text{sym.} & & 245.83 & -3.72\\ & & & & 245.87\end{bmatrix}\times10^{-9}$
4	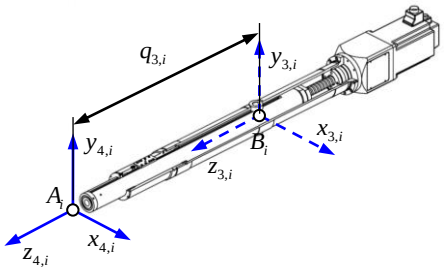 Limb-body assembly (including the P joint and the first R joint of the S joint)	$\boldsymbol{R}_{4,i}=\boldsymbol{R}_{3,i}=\left[\hat{\boldsymbol{x}}_{4,i}\quad\hat{\boldsymbol{y}}_{4,i}\quad\hat{\boldsymbol{z}}_{4,i}\right]$, $\boldsymbol{s}_{3,i}=\boldsymbol{s}_{4,i}=\hat{\boldsymbol{z}}_{4,i}$ $\boldsymbol{K}_{4,i}^{-1}=\begin{bmatrix}c_{4,i,11} & 0 & 0 & 0 & c_{4,i,15}\\ & c_{4,i,22} & 0 & c_{4,i,24} & 0\\ & & c_{4,i,33} & 0 & 0\\ & \text{sym.} & & c_{4,i,44} & 0\\ & & & & c_{4,i,55}\end{bmatrix}\times10^{-9}$
5	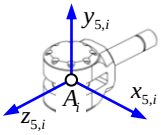 Second R joint of the S joint	$\boldsymbol{R}_{5,i}=\boldsymbol{R}_{4,i}\mathrm{Rot}\left(z_{4,i},\theta_{4,i}\right)=\left[\hat{\boldsymbol{x}}_{5,i}\quad\hat{\boldsymbol{y}}_{5,i}\quad\hat{\boldsymbol{z}}_{5,i}\right]$, $\boldsymbol{s}_{5,i}=\hat{\boldsymbol{y}}_{5,i}$ $\boldsymbol{K}_{5,i}^{-1}=\begin{bmatrix}6.48 & -1.50\times10^{-3} & 4.65\times10^{-3} & 1.23\times10^{-2} & -0.26\\ & 10.08 & 4.08\times10^{-3} & -110.26 & -0.17\\ & & 1.34 & 1.79\times10^{-2} & 4.10\times10^{-2}\\ & \text{sym.} & & 4.62\times10^{3} & 6.05\\ & & & & 7.57\times10^{3}\end{bmatrix}\times10^{-9}$
6	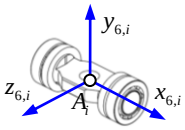 Third R joint of the S joint	$\boldsymbol{R}_{6,i}=\boldsymbol{R}_{5,i}\mathrm{Rot}\left(y_{5,i},\theta_{5,i}\right)=\left[\hat{\boldsymbol{x}}_{6,i}\quad\hat{\boldsymbol{y}}_{6,i}\quad\hat{\boldsymbol{z}}_{6,i}\right]$, $\boldsymbol{s}_{6,i}=\hat{\boldsymbol{x}}_{6,i}$ $\boldsymbol{K}_{6,i}^{-1}=\begin{bmatrix}2.43 & -1.72\times10^{-3} & -1.79\times10^{-4} & -3.60\times10^{-2} & 4.75\times10^{-2}\\ & 5.66 & 2.35\times10^{-3} & -0.24 & 0.17\\ & & 1.93 & -1.73\times10^{-2} & 0.18\\ & \text{sym.} & & 1.08\times10^{3} & 1.21\\ & & & & 2.54\times10^{3}\end{bmatrix}\times10^{-9}$

$\hat{\boldsymbol{x}}_{m_i,i}$, $\hat{\boldsymbol{y}}_{m_i,i}$ and $\hat{\boldsymbol{z}}_{m_i,i}$ are unit vectors of the three orthogonal axes of $\{R_{m_i,i}\}$ evaluated in $\{R\}$; $\boldsymbol{E}_3$ is an identity matrix of order three. The modulus of elasticity and Poisson ratio of the material used in the m_ith ($m_i=1\sim6$) component are: E=2.06×10^{11} Pa , μ=0.27 .

Table A-2 The body fixed frames and compliance matrixes of the elastic elements in the passive limb

m_4	$\{R_{m_4,4}\}$	$\boldsymbol{R}_{m_4,4}$, $\boldsymbol{s}_{j_4,4}$, $\boldsymbol{K}_{m_4,4}^{-1}$ (unit: N, m, rad)
1	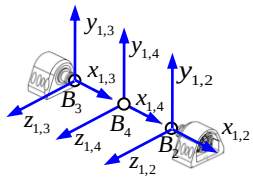 R joint	$\boldsymbol{R}_{1,4}=\boldsymbol{E}_3=\left[\hat{\boldsymbol{x}}_{1,0}\quad\hat{\boldsymbol{y}}_{1,0}\quad\hat{\boldsymbol{z}}_{1,0}\right]$ $\boldsymbol{R}_{1,2}=\boldsymbol{R}_{1,3}=\boldsymbol{R}_{1,4}$, $\boldsymbol{s}_{1,4}=\hat{\boldsymbol{z}}_{1,4}$, $\boldsymbol{s}_{1,2}=\boldsymbol{s}_{1,3}=\boldsymbol{s}_{1,4}$ $\boldsymbol{K}_{1,4}^{-1}=\begin{bmatrix}0.50 & -3.78\times10^{-4} & -4.35\times10^{-4} & -1.14\times10^{-3} & -4.21\times10^{-3}\\ & 2.51 & -8.09\times10^{-4} & 3.92\times10^{-3} & -8.76\times10^{-3}\\ & & 2.95 & 7.65\times10^{-3} & -1.17\times10^{-3}\\ & \text{sym.} & & 1.95 & 2.77\times10^{-3}\\ & & & & 1.72\end{bmatrix}\times10^{-9}$
2	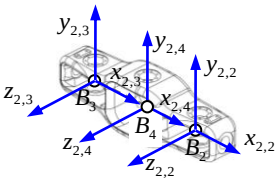 Base link	$\boldsymbol{R}_{2,4}=\boldsymbol{R}_{1,4}\mathrm{Rot}\left(x_{1,4},\theta_{1,4}\right)=\left[\hat{\boldsymbol{x}}_{2,4}\quad\hat{\boldsymbol{y}}_{2,4}\quad\hat{\boldsymbol{z}}_{2,4}\right]$ $\boldsymbol{R}_{2,2}=\boldsymbol{R}_{2,3}=\boldsymbol{R}_{2,4}$ $\boldsymbol{K}_{2,4}^{-1}=\begin{bmatrix}\boldsymbol{C}_{2,4,22} & \boldsymbol{C}_{2,4,23} & \boldsymbol{C}_{2,4,24}\\ & \boldsymbol{C}_{2,4,33} & \boldsymbol{C}_{2,4,34}\\ \text{sym.} & & \boldsymbol{C}_{2,4,44}\end{bmatrix}$
3	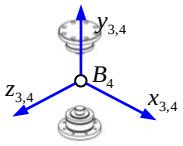 R joint of RP limb	$\boldsymbol{R}_{3,4}=\boldsymbol{R}_{2,4}\mathrm{Rot}\left(y_{2,4},\theta_{2,4}\right)=\left[\hat{\boldsymbol{x}}_{3,4}\quad\hat{\boldsymbol{y}}_{3,4}\quad\hat{\boldsymbol{z}}_{3,4}\right]$, $\boldsymbol{s}_{2,4}=\hat{\boldsymbol{y}}_{3,4}$ $\boldsymbol{K}_{3,4}^{-1}=\begin{bmatrix}0.83 & 1.44\times10^{-4} & -1.76\times10^{-3} & 5.07\times10^{-2} & -3.12\times10^{-2}\\ & 1.75 & 8.14\times10^{-4} & -9.73\times10^{-3} & 9.46\times10^{-3}\\ & & 0.83 & 5.07\times10^{-2} & -5.07\times10^{-2}\\ & \text{sym.} & & 56.52 & 0.12\\ & & & & 56.51\end{bmatrix}\times10^{-9}$
4	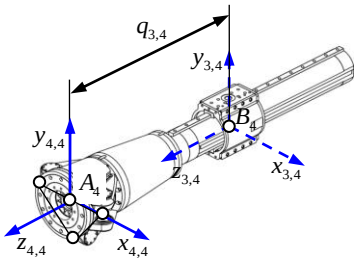 Limb-body assembly	$\boldsymbol{R}_{4,4}=\boldsymbol{R}_{3,4}=\left[\hat{\boldsymbol{x}}_{4,4}\quad\hat{\boldsymbol{y}}_{4,4}\quad\hat{\boldsymbol{z}}_{4,4}\right]$, $\boldsymbol{s}_{3,4}=\hat{\boldsymbol{z}}_{4,4}$ $\boldsymbol{K}_{4,4}^{-1}=\begin{bmatrix}c_{4,4,11} & 0 & 0 & c_{4,4,15} & 0\\ & c_{4,4,22} & c_{4,4,24} & 0 & 0\\ & & c_{4,0,44} & 0 & 0\\ & \text{sym.} & & c_{4,4,55} & 0\\ & & & & c_{4,4,66}\end{bmatrix}\times10^{-9}$
5	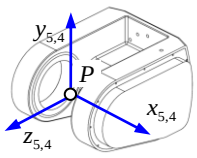 C-axis assembly	$\boldsymbol{R}_{5,4}=\boldsymbol{R}_{4,4}\mathrm{Rot}\left(z_{4,4},\theta_{4,4}\right)=\left[\hat{\boldsymbol{x}}_{5,4}\quad\hat{\boldsymbol{y}}_{5,4}\quad\hat{\boldsymbol{z}}_{5,4}\right]$, $\boldsymbol{s}_{4,4}=\hat{\boldsymbol{z}}_{5,4}$ $\boldsymbol{K}_{5,4}^{-1}=\begin{bmatrix}39.68 & -3.78\times10^{-2} & -0.20 & -1.95 & 1.34\times10^{2} & -22.77\\ & 47.09 & 5.15\times10^{-3} & -1.67\times10^{2} & -0.15 & -1.16\\ & & 2.17 & -1.36 & 0.14 & -0.57\\ & & & 7.08\times10^{2} & -11.46 & -11.90\\ & \text{sym.} & & & 5.49\times10^{2} & 12.88\\ & & & & & 3.50\times10^{3}\end{bmatrix}\times10^{-9}$
6	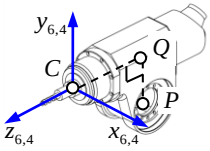 A-axis assembly	$\boldsymbol{R}_{6,4}=\boldsymbol{R}_{5,4}\mathrm{Rot}\left(x_{5,4},\theta_{5,4}\right)=\left[\hat{\boldsymbol{x}}_{6,4}\quad\hat{\boldsymbol{y}}_{6,4}\quad\hat{\boldsymbol{z}}_{6,4}\right]$, $\boldsymbol{s}_{5,4}=\hat{\boldsymbol{x}}_{6,4}$ $\boldsymbol{K}_{6,4}^{-1}=\begin{bmatrix}8.97 & -1.20 & -0.28 & 4.49 & 34.23 & -18.41\\ & 89.53 & -57.51 & -4.87\times10^{2} & -4.33 & 5.10\\ & & 39.11 & -3.16 & -1.61 & -0.84\\ & & & 2.96\times10^{3} & 24.61 & -9.73\\ & \text{sym.} & & & 4.68\times10^{2} & -11.73\\ & & & & & 4.50\times10^{2}\end{bmatrix}\times10^{-9}$

$\hat{\boldsymbol{x}}_{m_4,4}$, $\hat{\boldsymbol{y}}_{m_4,4}$ and $\hat{\boldsymbol{z}}_{m_4,4}$ are unit vectors of the three orthogonal axes of $\{R_{m_4,4}\}$ evaluated in $\{R\}$. The modulus of elasticity and Poisson ratio of the material used in the m_4th ($m_4=1\sim4$) component are: E=2.06×10[11] Pa, μ=0.27; and for the material used in the 5th and 6th component, the modulus of elasticity and Poisson ratio of the are: E=0.69×10[11] Pa, μ=0.33.

Table A-3 Structural parameters of the limb-body assemblies

	The geometry of the component	Parameters (unit: m)
Actuated limb	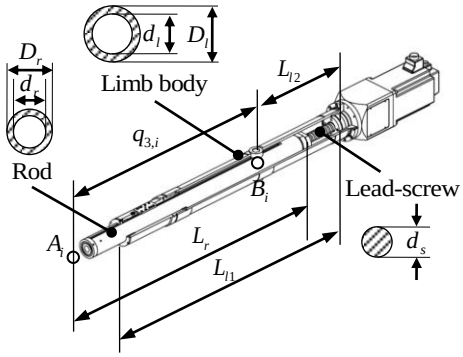	(1) Lead-screw: diameter $d_s = 0.028$; (2) Rod: length $L_r = 0.9$; diameter $D_r = 0.06$, $d_r = 0.04$; (3) Limb body: lengths $L_{l1} = 0.83$, $L_{l2} = 0.36$; diameters $D_l = 0.09$, $d_l = 0.075$.
Passive limb	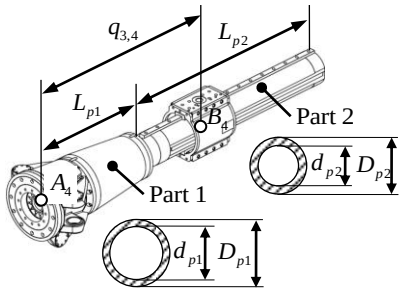	(1) Part 1: length $L_{p1} = 0.45$; diameters $D_{p1} = 0.21$, $d_{p1} = 0.194$; (2) Part 2: length $L_{p2} = 0.92$; diameters $D_{p2} = 0.13$, $d_{p2} = 0.106$.

In Table A-1:

$$
\begin{aligned}
&c_{4,i,11} = \left(0.86q_{3,i}^3 + 2.60q_{3,i}^2 - 3.07q_{3,i} + 1.07\right)\times 10^3, \qquad c_{4,i,22} = \left(0.99q_{3,i}^3 + 1.88q_{3,i}^2 - 2.56q_{3,i} + 0.90\right)\times 10^3 \\
&c_{4,i,33} = \left(q_{3,i} + L_{l2} - L_r\right)/EA + 9.30, \quad L_r = 0.9, \quad L_{l2} = 0.36, \quad EA = 0.1293 \\
&c_{4,i,44} = \left(6.91q_{3,i}^3 - 19.45q_{3,i}^2 + 24.51q_{3,i} - 2.45\right)\times 10^3, \qquad c_{4,i,55} = \left(11.36q_{3,i}^3 - 31.34q_{3,i}^2 + 34.73q_{3,i} - 5.01\right)\times 10^3 \\
&c_{4,i,15} = \left(-34.57q_{3,i}^3 + 13.26q_{3,i}^2 - 10.36q_{3,i} + 3.26\right)\times 10^3, \quad c_{4,i,24} = \left(32.59q_{3,i}^3 - 12.57q_{3,i}^2 + 9.87q_{3,i} - 3.02\right)\times 10^3
\end{aligned}
\tag{A-1}
$$

In Table A-2:

$$
\boldsymbol{C}_{2,4,,22} = \begin{bmatrix}
0.26 & -5.30\times10^{-4} & -2.87\times10^{-5} & 1.51\times10^{-2} & 1.47\times10^{-4} & -1.21\times10^{-3} \\
 & 1.83 & -2.34\times10^{-3} & 3.96\times10^{-2} & -1.68\times10^{-2} & -3.97 \\
 & & 1.05 & 6.45\times10^{-3} & 4.05 & 5.17\times10^{-3} \\
 & & & 135.87 & -5.24\times10^{-3} & -2.97\times10^{-2} \\
 & \text{sym.} & & & 41.71 & 4.46\times10^{-2} \\
 & & & & & 32.14
\end{bmatrix}\times10^{-9} \tag{A-2}
$$

$$
\boldsymbol{C}_{2,4,,33} = \begin{bmatrix}
0.26 & 3.94\times10^{-4} & 2.22\times10^{-4} & 2.97\times10^{-3} & -1.84\times10^{-3} & -1.17\times10^{-4} \\
 & 1.83 & 3.87\times10^{-3} & 4.65\times10^{-3} & -2.51\times10^{-2} & 3.98 \\
 & & 1.05 & -3.88\times10^{-3} & -4.06 & -2.03\times10^{-4} \\
 & & & 136.03 & 2.34\times10^{-2} & 9.91\times10^{-3} \\
 & \text{sym.} & & & 41.75 & -1.04\times10^{-2} \\
 & & & & & 32.18
\end{bmatrix}\times10^{-9} \tag{A-3}
$$

$$\boldsymbol{C}_{2,4,44}=\begin{bmatrix} 0.29 & -7.17\times10^{-4} & 5.34\times10^{-5} & 1.20\times10^{-2} & -1.94\times10^{-3} & 6.14\times10^{-3} \\ & 3.84 & 2.00\times10^{-3} & 4.93\times10^{-2} & 1.25\times10^{-2} & -1.33\times10^{-2} \\ & & 2.81 & -9.22\times10^{-3} & 1.00\times10^{-2} & -1.95\times10^{-2} \\ & & & 196.16 & -1.60\times10^{-2} & -4.28\times10^{-2} \\ & \text{sym.} & & & 25.31 & -1.17\times10^{-2} \\ & & & & & 17.30 \end{bmatrix}\times10^{-9} \tag{A-4}$$

$$\boldsymbol{C}_{2,4,23}=\begin{bmatrix} 754\times10^{-2} & -7.22\times10^{-4} & -2.69\times10^{-4} & 7.32\times10^{-3} & 1.25\times10^{-3} & 3.83\times10^{-4} \\ 8.36\times10^{-5} & 0.56 & 8.9\times10^{-4} & 1.87\times10^{-2} & -5.04\times10^{-3} & 1.30 \\ 1.74\times10^{-4} & -2.17\times10^{-3} & 0.80 & 1.69\times10^{-3} & -3.13 & -9.79\times10^{-3} \\ 4.74\times10^{-3} & 3.02\times10^{-2} & -2.29\times10^{-3} & 58.80 & 1.11\times10^{-2} & 5.72\times10^{-2} \\ 2.23\times10^{-3} & -8.44\times10^{-4} & 3.13 & -3.96\times10^{-2} & -19.31 & -5.73\times10^{-2} \\ 2.68\times10^{-4} & -1.29 & -8.27\times10^{-3} & -1.54\times10^{-3} & 4.76\times10^{-2} & 4.33 \end{bmatrix}\times10^{-9} \tag{A-5}$$

$$\boldsymbol{C}_{2,4,24}=\begin{bmatrix} 0.16 & -1.50\times10^{-3} & -4.47\times10^{-4} & 5.80\times10^{-3} & 2.73\times10^{-4} & 7.06\times10^{-4} \\ -7.86\times10^{-4} & 1.71 & -5.86\times10^{-4} & 3.94\times10^{-2} & 7.67\times10^{-3} & 0.60 \\ 1.14\times10^{-5} & -1.26\times10^{-3} & 1.28 & 4.62\times10^{-3} & -1.16 & -1.16\times10^{-2} \\ 1.11\times10^{-2} & 4.14\times10^{-2} & 2.52\times10^{-3} & 116.31 & -2.14\times10^{-2} & -2.95\times10^{-2} \\ 2.16\times10^{-3} & -7.21\times10^{-3} & 7.59 & -6.58\times10^{-2} & -4.67 & -6.98\times10^{-2} \\ 3.79\times10^{-3} & -3.60 & -2.15\times10^{-3} & -4.11\times10^{-2} & -4.06\times10^{-2} & 9.69 \end{bmatrix}\times10^{-9} \tag{A-6}$$

$$\boldsymbol{C}_{2,4,34}=\begin{bmatrix} 0.16 & 7.23\times10^{-4} & 4.62\times10^{-4} & 3.80\times10^{-3} & -3.41\times10^{-4} & 1.66\times10^{-3} \\ -2.55\times10^{-4} & 1.70 & 1.80\times10^{-3} & 4.54\times10^{-2} & 1.24\times10^{-2} & 0.60 \\ -1.62\times10^{-4} & 3.78\times10^{-3} & 1.28 & -8.64\times10^{-3} & -1.17 & -1.36\times10^{-2} \\ 9.59\times10^{-3} & 1.20\times10^{-2} & -5.09\times10^{-3} & 116.27 & -7.69\times10^{-3} & 1.50\times10^{-2} \\ 8.68\times10^{-5} & -2.39\times10^{-2} & -7.61 & 5.79\times10^{-2} & -4.74 & 8.58\times10^{-2} \\ 4.86\times10^{-3} & 3.60 & -1.15\times10^{-2} & 8.89\times10^{-2} & 3.88\times10^{-2} & 9.68 \end{bmatrix}\times10^{-9} \tag{A-7}$$

$$\begin{aligned} &c_{4,4,11}=219.75q_{3,4}^3-145.08q_{3,4}^2+30.86q_{3,4}+3.24, && c_{4,4,22}=145.68q_{3,4}^3+0.22q_{3,4}^2-45.28q_{3,4}+20.41 \\ &c_{4,4,44}=1175.41q_{3,4}+554.43, && c_{4,4,55}=666.67q_{3,4}+760.83 \\ &c_{4,4,66}=-74.07q_{3,4}^3+219.05q_{3,4}^2+720.71q_{3,4}+507.67, && c_{4,4,15}=19.75q_{3,4}^3-382.86q_{3,4}^2+192.03q_{3,4}-29.29 \\ &c_{4,4,24}=27.16q_{3,4}^3+167.30q_{3,4}^2+25.58q_{3,4}-22.58 \end{aligned} \tag{A-8}$$